Ion Trapping by Dust Grains: Simulation Applications to the Enceladus Plume

W. M. Farrell[a], J.-E. Wahlund[b], M. Morooka[b], W. S. Kurth[c], D. A. Gurnett[c], and R. J. MacDowall[a]

a. NASA Goddard Space Flight Center, Greenbelt, MD, USA
b. Swedish Institute of Space Physics, Uppsala, Sweden
c. University of Iowa, Iowa City, IA, USA
031517;

Abstract: Using a particle-in-cell electrostatic simulation, we examine the conditions that allow low energy ions, like those produced in the Enceladus plume, to be attracted and trapped within the sheaths of negatively-charged dust grains. The conventional wisdom is that all new ions produced in the Enceladus plume are free to get picked up (i.e., accelerated by the local E-field to then undergo vB acceleration). However, we suggest herein that the presence of submicron charged dust in the plume impedes this pickup process since the local grain electric field greatly exceeds the co-rotation E-fields. The simulations demonstrate that cold ions will tend to accelerate toward the negatively charged grains and become part of the ion plasma sheath. These trapped ions will move with the grains, exiting the plume region at the dust speed. We suggest that Cassini's Langmuir probe is measuring the entire ion population (free and trapped ions), while the Cassini magnetometer detects the magnetic perturbations associated with pickup currents from the smaller population of free ions, with this distinction possibly reconciling the ongoing debate in the literature on the ion density in the plume.

- The Enceladus plume contains neutrals, newly-formed ions, & dust and the dust can influence ion trajectories
- Without dust, ions are free to get picked-up by the local corotating magnetoplasma
- Our simulations show that with added dust, the large E-fields from the grain charge disrupts pick-up and creates ion trapping

I. Introduction

A surprising observation from the Cassini mission to Saturn is the detection of substantial gas and particulate plumes emitted from the south pole of Saturn's moon Enceladus (Porco et al., 2006; Waite et al., 2006; Hansen et al., 2006; Dougherty et al., 2006; Spahn et al., 2006). The jets originate from fissures cutting across the polar region (Porco et al., 2006) and the associated gas emission is found to be mostly composed of water (90%), CO_2 (5%), and traces of various hydrocarbons (Waite et al., 2009). The jets also possess large concentrations of charged salty-ice dust (Spahn et al., 2006; Postberg et al., 2009). There have been over 20 flybys of the moon/plume system.

While the understanding of the neutral gas densities and plume dynamics are coming into focus, there is the very interesting development of a dilemma in the observed plume-created ion concentrations. Specifically, the Cassini magnetometer detected a magnetic field perturbation (Dougherty et al., 2006) consistent with ion pickup currents on the order of 10^5 A. High quality detailed hybrid plasma simulations of the pickup process (Kriegel et al., 2009, 2011, 2014; Meier et al., 2014) suggest that plume ion densities of <3000 ions/cm^3 can account for the detailed structure in the B-field magnitude and orientation. The model B-field from plume pick-up ions and measured B-field are remarkably close. In contrast, during the same encounters, the Cassini Langmuir Probe (LP) that is part of the Radio and Plasma Wave Science (RPWS) instrument, detected peak ion densities near 30000 ion/cm3 for the E3 encounter and close to 100,000 ions/cm^3 for the similar north-south E5 pass (see Figure 5 of Morooka et al., 2011). If every LP-measured ion produced in the plume was free to undergo 'pick up' in the local radial E-field to ~30 km/s, the associated ion pickup current would be near 10 MA, creating an anomalously large magnetic field perturbation that is simply not detected by the magnetometer (Farrell et al., 2014). **Table 1** lists the peak plasma and dust properties for the E3 encounter inferred from the B-field (Kriegel et al., 2014, Meier et al., 2014) versus those from the LP (Morooka et al., 2011, Farrell et al., 2014).

The contrast in observations creates an obvious dilemma and reconciliation may lie in a better understanding of the electrostatic effects of the plume-created ions in the pervasive dust environment in the plume. Such electrostatic effects include the development of plasma sheaths

about dust grains that act to trap newborn cold plume ions. Such dust-plasma effects have not been included in past regional-scale hybrid simulations.

Figure 1 illustrates the situation. Specifically, the neutral gas (i.e., water-based molecules) ionizes via photo-ionization, charge exchange (Johnson et al., 2006) and impact ionization at a rate, ν. Thus, there is a source of cold ions in the plume defined as, $S = \partial n_{w+}/\partial t = \nu n_w$ with $\nu \sim 2 \times 10^{-7}$/s (Johnson et al., 2006). However, if we drew a sphere about the plume of radius R of approximately an Enceladus radius of 250 km, the newly-formed ions would be lost out this sphere by transport at a rate of $L = n_{w+} \langle v \rangle / R$, where $\langle v \rangle$ is the average transport speed of the ions through the sphere boundary, R is the sphere radius, and nominal transport time as $\sim R/\langle v \rangle$. In the steady state, these two terms must balance, $dn_{w+}/dt = 0 = S - L$, thereby defining a general plume steady-state ion density as $n_{w+} \sim \nu n_w R/\langle v \rangle$. The presence of such newly-minted cold water ions has been reported by Tokar et al. (2009) and Morooka et al. (2011).

One can now see the dilemma: If the new ions in the plume, initially moving at < 1 km/s are all picked up to the corotation speed of $\langle v \rangle \sim 30$ km/s to move out of the sphere in the co-rotation direction (as illustrated in Figure 1), and $n_w \sim 5 \times 10^8/cm^3$ (as measured by the Cassini Ion and Neutral Mass Spectrometer, see Figure 8 Teolis et al. (2010)), we find the steady state plume-originating ion density is only $n_{w+} \sim 1000$ ions/cm^3, consistent with the ion densities inferred via the magnetometer (Kriegel et al., 2014).

However, if a large fraction of these newly-minted plume ions get entrapped in the sheath of the submicron dust grains, they will not get picked up and will effectively remain slow, moving at the speed of the dust grain at a few hundred meters per second ($\langle v \rangle \sim 500$ m/s). The dust grains charge to values between -0.5 to -6 V (Morooka et al., 2011; Dong et al., 2015), and for a ½-m Debye length [Morooka et al., 2011; Shafiq et al., 2011], the local E-fields from the randomly spaced dust approach values near 10 V/m. These random dust-created E-fields could impede or disrupt the pickup process, at least for low energy ions.

For example, consider a scenario presented previously [Farrell et al., 2014] where 97% of the ions get entrapped in the sheaths of dust grains, which themselves leave the near-plume region at ~500 m/s, then the steady state ion density via the continuity equation (i.e., $n_{w+} = \nu n_w R/\langle v \rangle$) is $n_{w+} \sim 50{,}000$ ions/cm^3, consistent with LP-measured values. Assuming the remaining 3% of the ions possess an energy that exceeds the sheath trapping potentials, then about 1500

ions/cm^3 are energetic enough (i.e., 'free') to get picked up to create the ion pickup current, more consistent with the densities inferred from the B-field perturbation.

In other words, the submicron dust and associated ion trapping could be the cause of the apparent observational dilemma. We suggest herein that there are two ion components: 1) a substantial population of trapped ions measured by the LP and 2) a smaller population of 'free' ions that affect the perturbation in B.

Figure 2 illustrates the effect of the charged dust grains on ion sheath formation. This figure is adapted from Figure 13 of Wahlund et al. (2009) who previously discussed low energy ion trapping in grain sheaths in the E-ring. Dust grain plasma sheaths create local perturbations in the plasma potential profile, with local excursions to values below -5 V (see Figure 6 of Dong et al., 2015). If new plume ions are initially injected at low energy, they will get trapped in these dust grain potential wells. For ions trapped in plasma sheaths about individual grains, a structure forms that is analogous to a plasma wave instability-created 'water-bag' feature in phase space plots (Figure 7-13 and 7-24 of Chen, 1984). These micro-potential wells contain ions that effectively orbit about the grain in a modified central potential about the center of the well. These trapped ions will have a velocity of $v_x = 0$ at the well edge (where they are turned around) and maximum velocity in the well center. When plotting ion velocity as a function of position, these water-bag like structures in phase space provide evidence of trapping.

The Enceladus plume is considered "rich" in dust, with direct detection of micron-sized grains (Spahn et al., 2006) and also the direct detection of 'nanograins' of a few nanometers in radius (Jones et al., 2009; Hill et al., 2012, Dong et al., 2015). Using the Langmuir Probe, Shafiq et al. (2011) also inferred that submicron grains from 30-100 nanometers must also be present in large quantities in order to explain the loss of electrons in the plume plasma, with the LP-measured ratio of electron-to-ion density, n_e/n_i, being as low as 0.03 in the central plume region. They argued that in equilibrium, the electrons are absorbed onto the submicron grains such that ~ 30 nm grains can maintain ~100-400 *e* of negative charge (Farrell et al., 2014). As shown in Table 1, local charge neutrality is maintained by including the negative charge on the ~100 submicron grains/cm^3 in the plume region (Shafiq et al., 2011; Morooka et al., 2011; Dong et al., 2015). In order to maintain local neutrality, ion sheaths also of 100-400 *e* positive charge should also form around these submicron grains.

One can picture a very complicated micro-potential structure in the Enceladus plume, with numerous, highly local negative dust grain potential wells of various depths associated with grains of micron to submicron sizes (e.g., Figure 4 of Goertz (1989)). In essence, the sub-corotational E-field in and about the plume at milliVolts per meter levels that would otherwise initiate the ion pickup process would be overpowered/disrupted by the large quasi-random noise, $\Delta E \sim 1\text{-}10$ V/m, in association with the randomly-spaced dust sheaths. For low speeds ions, this ΔE would thus interrupt ion pickup and dominate the ion dynamics.

In this paper, we examine the conditions that will create dust trapping of ions using a 1D particle-in-cell plasma simulation code having negatively charged dust, electrons, and ions in the system. The simulation provides a demonstration of the trapping process, and the results are used to guide inferences regarding the dusty plasma at Enceladus. The environmental ion population will be examined at various simulated temperatures (cold, cool, and warm). The ions are initially placed uniformly in the simulation and are all initially 'free'. However, if their energy is low enough, the ions will indeed get entrapped. At lowest simulated temperatures, substantial ion trapping is clearly evident. We find that as temperature increases the number of free ions increases; their presence evident in the resulting ion density profiles.

II. Simulation Model

We apply a 1D particle-in-cell code that has been used in the past to model the plasma expansion into the lunar wake (Farrell et al, 1998, 2008) and more recently to model the increase in the escape flux of photo-electrons from the lunar surface during a CME passage (Farrell et al., 2013).

In this present case, we apply periodic boundary conditions at simulation edges. We assume that simulation dimension is along the ambient B-field. The total number of negative and positive charges in the simulation remain balanced (the system is charge-neutral). However, we form negatively charged dust grains by 'bunching' individual simulated electrons into concentrations located at specific pre-defined locations in the simulation. These electron bunches can also be given a 'dust velocity' such that they can move in the simulation, but initially they are stationary and uniformly spaced (Δx) along the simulated x direction. We can vary the number of electrons in a 'bunch' (i.e., on the dust grain) from 1% to 100% of the electron content in the surrounding 2 Debye length region about the grains. We will compare results from as many as 9 different runs, so we optimize for speed: In order to speed up the effects, we assume the simulated ion mass is 20 times the electron mass, which will act to make the ions appear more energetic than they really are at Enceladus. However, this alteration is performed to allow the simulations to be run in a reasonable time span. While the simulations might reveal some extra detail in 2 dimensions, we in fact can show the requirements for the development of ion sheath formation about grains using only a 1D code that assumes ion mobility along the ambient magnetic field line – and this choice further optimizes simulation run times. We then run cases under varying simulated ion temperatures, defining a cold ion thermal speed, v_{ti}, as $v_{te}/45$ (or 45 times smaller than the electron thermal speed, v_{te}), cool ion thermal speed at $v_{te}/9$ and warm thermal speed at $v_{te}/5$.

We note that in the Enceladus plume, the electrons have a temperature near 2-3 eV, making $v_{te} \sim 900$ km/s. In contrast, the newly minted ions in the plume likely have speeds near 1 km/s. Thus, the real thermal speed ratios, v_{ti}/v_{te} are 1/900 and the plume ions are much colder than modeled here. We consider this simulation a demonstration of the possibility of trapping, and even cooler temperatures associated with newborn ions should create greater trapping.

When there is strong ion trapping near a dust grain, the plot of ion concentration in a x vs t format (e.g., Figure 3) creates vertical stripes since the ions concentrate in the sheaths of the equally-spaced negative dust grains. This visual effect, appearing as a 'picket fence' in the x vs t plot, is the signature of strong trapping/sheath formation.

We run the simulations for the early period in the dust-ion interactions – in the first 200 plasma periods when the sheaths first form. We specifically are targeting this early time when initially free ions interact with negative charged bunches (dust grains) to form the sheaths. On these short time scales, we assume that the initial charge in the bunch (or the charge on the grain) stays constant (see further discussion in Section IV). For longer times, dust grains will alter their charge state as the plasma and surrounding charged dust environment changes. For example, in and near the Enceladus plume, submicron grain charging reaction times are on the order of 10-100 seconds (Farrell et al., 2012; Dong et al., 2015). In this environment, the charge state of the submicron grains is changing on time scales substantially longer than those modeled herein. Thus, we assign each electron bunch/dust grain a charge state that conserves system-level equilibrium (number of free electrons and bunch-bound electrons equals the number of ions in the system) but not local equilibrium in the few Debye-length neighborhood about the bunch/grain. We then allow the free electrons and free ions to reconfigure themselves under the electrical influence of the bunches/dust grains to determine ion sheath formation as a function of grain charge, grain configuration, and ion thermal velocity.

We note that hybrid simulations typically do not include these grain-scale electrostatic effects, like ion trapping and sheath formation. Meier et al. (2014) conceived of a clever new nano-grain charging module incorporated into a hybrid code. The small grains of < 10 nm were allowed to charge under the influence of the local simulated plasma environment, and were then treated as a single-charged heavy ion in the simulation to self-consistently add to the plasma density, currents, E-fields and B-fields in the system. This new approach produced a simulated charged nano-grain profile that closely matched that observed by the Cassini Plasma Spectrometer (CAPS) (Jones et al., 2009; Hill et al., 2012). They modeled grains of less than 10 nm in size and did not include the charging and ion sheath formation in the larger submicron grain population between 10-500 nm. We thus now use our 1D PIC code as a demonstration of grain-plasma sheath formation for larger grains (10-500 nm) but applied in a limited space

198 (~many 10's of meters). We then use the model results to further interpret the Cassini/Enceladus
199 observations.
200 The plume is considered weakly-collisional: Over the scale size of the plume (~ 2-3
201 Enceladus radii), there is a likelihood of collisions especially of electrons and ions with the
202 neutral water molecules. The mean free path for an electron-water molecule collision is
203 approximately 10 kilometers and the collision frequency is about 100 Hz – well below the
204 electron plasma frequency. Ion-neutral collision frequencies are substantially less (by a factor of
205 200 or so). We do not consider the effect of these collisions herein since the collision frequency
206 is less than the electron plasma frequency. Past PIC codes of terrestrial upper-atmosphere
207 charged particle motion have included such collisions as a bulk drag force on electron and ion
208 motion. However, the collisions are so infrequent, any inclusion of such effects would likely
209 have to be in the form of a Monte Carlo quasi-random change in motion of randomly-selected
210 electrons and ions. This addition to that specific coding is unnecessary especially for considering
211 the creation of a trapped ion population about dust grains.
212 Within the plume, there are also electron and ion collisions with the charged dust (or very
213 localized electrostatic fields associated with dust) and these plasma-dust collisional effects are
214 exactly the ones being modeled herein. This code is specifically designed to obtain a greater
215 understanding of the electron-dust and ion-dust 'collisional' effects, especially given the trapping
216 E-fields of the charged. dust that alter ion dynamics on the small scale.
217
218

III. Results

Figure 3 shows the results of the ion dynamics as a function of time in two extreme cases. Specifically, the E-field and ion density are plotted as a function of position (x, plotted horizontally from 0 to 100 Debye length) and time (plotted vertically in the first 150 plasma periods). We initially place 16 equally-spaced dust grains in the simulation, with the panels on the left displaying E(x) and $n_i(x)$ for dust charged with only1% of the surrounding electrons and with warm ion thermal speeds. We expect little trapping and indeed little trapping is evident with ion densities showing only thermal fluctuations (as if the electron bunch/charged dust was not present in the simulation). In this case, most of the ions are 'free' and we would expect nearly all ions to move in bulk under the influence of a co-rotation E-field. However, the panels on the right also display E and n_i but now with increased dust charge concentrations to 98% of the surrounding (2 Debye length) electron content and now with cold ion thermal speeds. While the ions are initially placed in the simulation free and unbounded, they very quickly congregate to the negative dust concentrations, forming long-lasting ion density enhancements in the form of ion sheaths about the grain (as evident in the vertical stripes in the lower right panel). The associated E-field also displays obvious structure associated with the dust potentials. In both E and n_i, the 'picket fence' signature of strong ion trapping is clearly present.

A careful examination of the right-hand panels of Figure 3 reveals an initial modulation in both the E-field and ion sheath. Specifically, in the E-field panel in the upper right, we note that about 10-20 plasma periods into the simulation, the E-field 'picket fence' structures for a brief period disappear (the 'blurred' layer near the bottom of the panel). At the same time, the ion densities are at their largest concentrations. At this early point, the initially-free ions have all spatially moved to merge and surround the negative charge cluster to thus create near perfect neutrality. However, the motion in the sheath ions is similar to a harmonic oscillator, and the moment of near-perfect neutrality is lost as many of these sheath ions then move past their central site to spread to their largest spatial separation from the negative dust grain in the sheath. This oscillatory nature continues over then next few 10's of plasma periods (see the periodic intensifying and 'blurring' effect in the ion densities in the lower right panel) and eventually this effect damps out. Recall in the derivation of the electron plasma frequency, a common analytical

approach is to displace a slab of electrons and let them oscillate about the more massive, stationary positive ion charge (see page 11 of the Gurnett and Bhattacharjee, 2005). We note in our simulation, that now includes large negative dust grains, that the ions are now the lighter, less massive charge species compared to the dust grains. Thus, the ions are now undergoing an analogous oscillatory motion about the quasi-stationary negative grains.

Figure 4 is a more thorough parameter examination of the evolution of ion density as a function of dust grain charge and ion temperature. Each individual panel shows ion density as a function of x (horizontally, 0 to 100 Debye Lengths) and time (vertically, 0 to 150 plasma periods) in an identical format to Figure 3. If trapping is evident, it would present itself as enhanced ion concentrations (i.e., the picket fence morphology in the x vs t plots.)

As with Figure 3, for low dust grain charge and warm ion thermal velocities (lower left), the ions behave as if the dust is not present and we find mobile ions that possess thermal fluctuations. Such unbounded ions would be free to get picked up by the weak co-rotation E-field. However, as dust charge increases, there is progressively more trapping of the ions, with the most extreme case occurring for substantial dust charging and cold ion temperatures (upper right). We note that sheath formation and ion trapping is evident even for warm ions in the case when the dust is highly charged. However, the trapping structures are more diffuse and there is an increase in the background 'free' ion level. In the real Enceladus plume, the newly-minted ions temperatures are low, more similar to the cold case in the upper right corner of Figure 4.

Figure 5 shows the results of the simulation for 50 grains in the simulation box (in 100 Debye lengths) with grains randomly spaced and randomly charged. This situation is most similar to the Enceladus plume where grains from micron to submicron sizes have local potential wells of various depth and quasi-random spacing. We again show x (0-100 λ_D) versus time (0-150 ω_{pe}^{-1}) for (a) electron density, (b) E-field, and (c) ion density. The electron density includes both free electrons and those electrons pre-defined to be 'bunched' to form the dust grains. As such, the panel on the right of electron density actually reveals the location and charge level of the dust grains themselves. Given that we randomized dust position and charge state, this plot provides the electrostatic context for the simulation. As indicated in Figure 5a, because of the random nature, we naturally form dust grain clusters where the inter-grain spacing is on the order of or less than 2 Debye lengths. These grain clusters are identified in Figure 5a.

In Figure 5b, the E-field associated with the dust grains is most pronounced for grains with the largest negative charge. Grains of lower charge also appear to have a ΔE associated with them but the E-field excursions are not as pronounced. However, very interesting micro-structure appears in the ion densities in Figure 5c. Ions are initially free but those near the dust feel the grain E-field: They migrate and remain (i.e., congregate) near the charged grains to form sheaths within the first few plasma periods (i.e., time scales of ~ 10 plasma periods). However, a careful examination of the regions near the dust clusters indicates that the trapped ion motion is indeed dynamic, with apparent 'ribbon' structures forming in x-vs-t ion density plots. These features are ions moving from grain to grain within the cluster. In essence, as grains in the cluster get within a few Debye lengths of each other, the walls defining the potential well that act to isolate trapped ion populations decrease, allowing the ions contained in individual sheaths to merge and hop across the lower inter-grain potential. As we show in Section IV, these ribbons are merging ion phase space water bag structures that extend between dust grains in close proximity.

Figure 6 shows a simulation run for 50 grains randomly spaced and randomly charged, but each grain is now given a random dust grain velocity. The panels are the same x-vs-t plots for (a) electron density (i.e., dust charge and position), (b) E-field, and (c) ion density as in Figure 5. As scaled, the dust grain velocity is actually much faster than dust speeds at Enceladus. However, the modeling exercise is revealing, especially in regions where the grains trajectories intersect and sheaths merge. Again, we note the development of ion ribbon structures in the ion density (Figure 6c) indicating ions 'jumping' from grain to grain. Where grains cross paths, their ion sheaths merge temporarily. We note that the electric field greatly intensifies at the edges of the merging regions.

Ions also appear to jump from grain sheath to grain sheath, and extending this to multi-dimensions, we can even consider this a form of cross-magnetic field conductivity. Given ions attached to the grains, the cross B-field plasma transport is an intrinsic by-product of dust movement. However, while there is significant bulk plasma transport associated with the moving grains, there is little net current because the positive ion sheath and negative charged dust migrate nearly quasi-neutral - with only a very slight charge imbalance in the slightly reduced positive sheath charge. Negatively charged dust pickup currents have been estimated for grains < 100 nanometers (Farrell et al., 2014; Dong et al., 2015). However, the overall net charge

310 (negative dust charge and their ion sheath) defining the net current is relatively small for the
311 electrically-shielded dust grains (Farrell et al., 2014).
312

IV. Phase Space Evidence of Ion Trapping

As discussed, if the new ions possess relatively low thermal velocities and become trapped in grain sheaths, then the x-vs-v plots should not only show density enhancements (i.e., picket fence structures) but also the classic water-bag like structures in phase space. **Figure 7** shows the ion phase space configuration for a single grain with Q_{dust}= 98%. The formation of a water-bag like structure is clearly evident. While the ions were initially injected with a random-normal distribution with a standard deviation of $v_{te}/45$ or ~0.02 v_{te}, the ions are locally accelerated in the potential wells of the dust grains and remain trapped in the (quasi-) central potential formed by the dust negative charge center. The ions appear to get 'heated' in the trapping process as they get accelerated into the trapping well. Without electrostatic energy loss, the ions would feel the influence of the potential but remain on escaping hyperbolic trajectories. However, electrostatic losses to surrounding particles via impulsive and wave activity dissipates energy and allows for trapping.

Pickett et al. (2015) reported on the presence of electrostatic solitary wave (ESW) structures in Saturn's inner magnetosphere that became nearly a factor of 100 times more intense in the Enceledus plume as compared to external regions (see their Figure 3). They report that in the plume there were three classes of RF micro-signatures: 1) dust impacts, 2) dust impacts with impact-generated plasma oscillation, and 3) clear and distinct solitary wave structures/bipolar pulses similar to those found in particle trapping regions/water bag structures of plasma wave activity. However, in the plume, these solitary structures were very intense – far more intense that in wave activity found away from the plume.

Given our simulation results, we suggest this third category of plasma wave micro-signatures, the ESWs, could be related to the antenna passing though the ion sheath of a relatively large dust grain. In other words, the grain did not impact the spacecraft to create an impulse, but the antenna was still capacitively-coupled to the fast-passing ESW that was in fact the grain sheath (e.g., Figure 7). The electric field associated with the ion sheath like that in Figure 7 is spatially bipolar – forming an ESW. Note also that the Debye length is ~0.5-1-m scale [Shafiq et al., 2011] and that the ion trapping feature extends about 3-5 Debye lengths. For a spacecraft traveling near 10-20 km/s, the change in E-field associated with the antenna transit

though the sheath-created ESW is about 0.05-0.1 millisecond duration – like that observed (see Figure 4 of Pickett et al. (2015)).

In the discussion section of Pickett et al. (2015) they suggest the 'unique plasma environment surrounding Enceladus could lead to generation of ESW's with higher amplitudes than found elsewhere…' . This conclusion is in agreement with our simulations: the dust-plasma interaction and the formation of ion sheaths may be the process behind these anomalously large ESW events detected in the plume.

The spacecraft, Cassini, is another solid object (like dust) in the plasma and is found to charge negative in the plume (Morooka et al., 2009; Dong et al., 2015). Cassini is moving at ~ 10-20 km/s through the plume and thus has an incident ion current about 3 times greater than the water ion thermal flux that would be incident at the surface of a low velocity dust grain. Despite the larger ion currents, the spacecraft is found to still charge negative. Our simulation results like Figure 5 and Figure 7 would suggest that the fast-moving spacecraft should also very quickly draw ions from the plasma (including ions trapped on other dust sheaths) and consequently develop its own unique ion trapping region - its own spacecraft ion sheath - about Cassini itself. Figure 7 shows that the cold plume ions are attracted to any negatively charged object of the approximate size of a Debye length (or less), suggesting the negatively charged spacecraft should develop its own trapped ion cloud. Thus, Figure 7 may explain the unusual energy broadened ion signatures detected by the Cassini Plasma Spectrometer (CAPS) during the E3 and E5 plume passages. Specifically Figure 2 of Tokar et al. (2009) shows ion energy spectrograms during Cassini's north–to-south transits past the moon. Initially at the plume entry, cold beams of ions are observed at distinct energy peaks in the 10's of eV associated with Cassini's incidence at ~14 km/s with nearly stationary newly-minted plume ions. However, deeper into the plume region, the initially cold beams get highly dispersed in energy – with the energy broadening extending from ~ 1 eV to ~10 eV. The Langmuir probe (Morooka et al. 2011; Dong et al., 2015) indicates that the spacecraft potential has large negative values (-2 to < -6 V) during these times, and this would be expected to create a near-spacecraft E-field in excess of 1 V/m. Our simulation indicates that such an E-field is capable of drawing the cold plume ions to the passing spacecraft. In essence, the broad ion population observed by CAPS is the newly-minted plume ions now trapped in the sheath of the spacecraft itself. Even though the spacecraft is fast-moving, it will still attract ions to form its own sheath.

Figure 8 and 9 show the results of two dust grains with Q_{dust} = 98% each moving towards each other at 0.1 times the electron thermal speed, which are allowed to merge in the simulation. The plasma ions are initially free and have a cold temperature ($v_{ti} = v_{te}/45$). Figure 8a shows the phase space configuration for early times just after the formation of the water-bag structures. We note that even though the grains are moving faster than the cold ion population, they will still attract ions and form ion-trapping sheaths (see also Figure 6 where fast moving dust grains clearly develop sheaths).

Besides these trapped ions, there is a portion of the ions that get accelerated moving as a precursor fast ion front. These are ions accelerated but not fully captured by the dust trapping potential. Note also the development of trailing secondary water bag structures that form in the wake of the dust grain. These trailing structures have some similarities to a Cerenkov disturbance, where the grains moving at constant velocities initiate plasma wave oscillations with the coupling mode to the plasma defined by an index of refraction varying with $\sim 1/v_{dust}$. These secondary water bag structures are likely related to dust-generated plasma wave activity. Figure 8b shows the time when the two dust grains and their sheaths merge. Ions from one initially-isolated sheath can now fully flow into the sheath of the other grain. The water bag structure appears very similar to that of a single grain (Figure 7), but now is more extended in velocity.

Figure 9 shows the evolution of the ion density as a function of position (100 Debye lengths) versus time (200 plasma periods) for Figure 8. While the ions are initially free, those in the vicinity of the grain feel the dominant attractive force from the negatively charged grain, to form the sheath. The fast precursor ions are evident and also the trailing disturbance is present as well as an apparent darker region (i.e., a trailing rarefaction).

A simulation run was also created using a cluster of 8 grains each separated by 4 Debye lengths. **Figure 10** shows the ion phase space configuration after 200 plasma periods, revealing the development of ion phase-space trapping and sheath formation about each of the grains. The simulation also reveals the presence of energetic escaping ions at $v > 0.2\ v_{te}$, these forming via scattering from their interaction with potential structures. These ions can be considered 'free' and would be the ones expected to be involved in pickup (see Section I). We anticipated the presence of the trapped ions in the dust potential wells, but the presence of the higher energy scattered population was initially a surprise. However, if we again rely on our analogy of particle trapping via plasma wave potentials, we should expect that there is a population of ions that would

undergo hyperbolic trajectories about the central grain potentials. These escaping ions also generate enhanced plasma wave activity as noted by the formation of ion trapping in plasma-wave created potentials. For example, such wave-trapped ions are found immediately adjacent to the set of grains in the outflow regions – like those between X = 10 to 20 Debye lengths.

Figure 11 shows the electron density in the vicinity of the cluster near the start of the simulation. By design, the negatively-charged dust is actually formed using electrons from the plasma population, and thus neutrality in the simulation is maintained. As electrons are removed from the plasma and added to the dust/bunch, there is a decrease in overall free electron content in the vicinity of the cluster, as indicated in the figure. While the simulation was purposely constructed to conserve total negative and positive charge, the figure illustrates the decreased electron concentrations in the vicinity of the cluster, similar to that observed by the Cassini Langmuir probe during the Enceladus transits (Wahlund et al., 2009; Shafiq et al., 2011; Morooka et al., 2011).

Figure 12 shows the ion density enhancements over 100 Debye lengths as a function of time during a 200 plasma period simulation run for the 8 grain cluster. While the ions initially were spaced homogenously in the simulation and were free to thermally migrate, those near the cluster form ion sheaths on time scales of 10 plasma periods. Also labeled is the outflow of more energetic ions from the cluster (which is a population that could undergo pickup). We also find that at the front of this energetic ion outflow there is a slight precursor disturbance in the form of an outward-traveling ion density depletion. Clearly, with the grain cluster, ions orbiting the negative charged grain undergo unusual accelerations under the perturbation of the nearby adjacent grains.

While the simulations presented herein are considered demonstrations to guide our thinking on the charged dust, ion, and electron dynamics, we suggest that Figures 10-12 are likely most applicable to the Enceladus situation. Specifically, each simulation Debye length represents ~ 0.5-1 m in the space environment in the Enceladus plume. As indicated in Table 1, in the plume, the Langmuir probe detected charge densities $\rho_i >> |\rho_e|$. To maintain neutrality, it was then inferred that there is a substantial population of submicron dust that provides a local negative charge density of $|\rho_d| = \rho_i - |\rho_e|$ [Shafiq et al., 2011]. We initially start the simulation herein with locally non-neutral conditions in the grain cluster, with dust charge densities dominating over ions and electrons in the few Debye lengths about the grains. However, after

10's of plasma periods, the plasma rearranges itself to obtain quasi-neutrality with the sheath forming about the grains to ensure $\rho_i \sim |\rho_d| >> |\rho_e|$.

However, we note that this quasi-neutrality is itself not perfect: As described in Section III and Figure 3, the ions in the sheath initially have their own oscillatory motion at the time of sheath formation, with the inner-sheath E-field and ion sheath concentrations modulated by this motion. Thus, the water bag structure/sheath structure itself undergoes its own maturation as these oscillations damp and the phase space configuration of ions becomes more evenly distributed.

The simulations are also run with light ions having 20 electron masses and the computed time for the light ions to become trapped is about 10 plasma periods. Scaling this to water-like ions at Enceladus, the trapping time is longer by a factor of the square root of the mass (or a factor of ~44) to near 400 plasma periods. We tested this by running the case in Figure 10 (8 grain cluster) using a mass difference between a 20 AMU ion and electrons of ~37000 and found identical structures developed in phase space but at nearly a factor of ~40 slower rate.

The 1D PIC code did not make a dynamic calculation for cases when there is more than one grain per Debye length. In this case, the code would have to account for mutual capacitive effects that lower the charge per grain dynamically. It is argued herein that on the time scales we are examining, the dust grains would not have time to dissipate or collect substantial charge to alter their overall charge state, and the charge state based on system-level neutrality at t= 0 would hold for the simulation runs of tens of thousands of plasma periods. However, in the future, any extended runs to times that scale to seconds should include dust charge dynamic effects including those associated with local plasma conditions and capacitive coupling to many grains per Debye sphere.

We thus purposely targeted early times in order to fully understand the evolution of the initially free ions into trapped sheath ions – and to demonstrate that cold newly minted ions will feel the strong pull from the nearby negatively charged dust grain over a weak sub-corotation E-field.

468 .

469

V. Conclusion

Our primary conclusion is the reconciliation of the observational dilemma of the ion concentrations in the Enceladus plume: The Cassini Langmuir probe is measuring a population of ions contained within the sheaths of negatively charged dust grains of > 10 nm in size. These sheath ions are not free to get picked up by the sub-corotational E-field, but instead exit the plume region in association with the dust. These trapped ions are moving relatively slowly - by a factor of 10-30 times more slowly than the free ions that get picked up and accelerated to speeds near 30 km/s. Thus, the steady-state density for the new plume ions will be large owing to their collectively slower plume exit speed (which is at the dust exit speed). However, we also recognize that some fraction of the ions have sufficiently high energies to remain free of the dust electrostatic trapping, and these ions likely contribute to the ion pickup current and associated perturbation in magnetic field detected by the Cassini magnetometer. The ratio of free-to-trapped ions is possibly only a few percent.

Our key simulation results applicable to the evolution of the new cold ions and dust sheath formation in the Enceladus plume are shown in Figure 4 and Figure 7, that demonstrate that new cold ions get accelerated toward and trapped within the near vicinity of the grain – and the local electrostatic forces in the grain-ion central potential dominate the dynamics of most of the low energy, trapped ions. Figures 8 and 10 show that dust-dust interactions can liberate and energize ions and this population is suspected to be that which ultimately gets picked up – with the free ions at a few percent of the total trapped ion population.

We conclude that the cause for the confusion in the interpretation of the observations is the presence of copious numbers of submicron particulates between 10-500 nm that, in equilibrium, are charged to many 100's of elementary negative charges. These grains possess substantial trapping ion sheaths. The nanograins of +/- 1 *e* (Jones et al., 2009; Hill et al., 2012) can be considered differently, somewhat similar to heavy negative and positive ions of +/- 1 *e*, which get picked up (Meier et al., 2014) but do not drag a substantial sheath with them. In contrast, the larger submicron grains should create randomly positioned and relatively deep potential wells that entrap the cold plume ion population. These ions then remain in trapped orbits about the dust grain and move in bulk with the grains. The Langmuir probe on Cassini

detects these trapped dust-sheath ions, but these ions will not contribute to the pick-up current measured by the Cassini magnetometer.

As described recently (Farrell et al., 2014), both the negative charge on the dust and its associated ion sheath exit the plume at the dust speed, v_{dust}, such that there is little net current associated with the moving dust. As such, the trapped ion component (the most substantial component) likely does not provide a significant perturbation to the ambient B field. In sharp contrast, the 2-3% of the overall ion population that is free to contribute to the pickup current has $J_i^{free} \sim n_i^{free} v_c e \sim 10^{-5}$ A/m^2 (with $n_i^{free} \sim$ 1000-3000/cm^3,corotation $v_c \sim 26$ km/s) and is unshielded by a corresponding electron current. This current creates a measurable B-field perturbation while the net current associated with the charge on the slow-moving dust is substantially smaller by a factor ~ 10 - 100 (Farrell et al., 2014).

The simulation results also lead to a new explanation for the intense electrostatic solitary structures/bipolar pulses reported in the Enceladus plume by Pickett et al. (2015). Figure 7, 8, and 10 all indicate that grain sheath regions form natural electrostatic solitary structures that could be detected by the Cassini radio system- especially if passing nearby a grain in an anomalously large charge state (within a few meters).

The simulations also provide a possible explanation for the ion energy broadening observed by CAPS (Toker et al., 2009) during the plume transit. In this case, the broadening is associated with newly minted low energy positive ions becoming entrapped in the sheath of the negatively-charged Cassini spacecraft itself.

Finally, we examined herein a limited region of space, ranging from a single Debye length to about 100 Debye lengths (0.5-50 m). We find there can be nested potential structures, with grain-ion interactions having a single-grain potential micro-well nested within a larger cluster well, and all contained in a regional plume potential well. This regional-scale E-field was not modeled herein (since we consider scale sizes of < 50 m) but would encompass a larger regional E-field system like that shown in Figure 4b and 4e of Meier et al. (2014). The interconnection of these nested potentials from small to regional scale has yet to be fully explored for the Enceladus plume.

The simulation results herein considered scales from the small to intermediate sizes, demonstrating the possible presence of large-scale dust sheath-related E-field micro-turbulence at 0.01-10 V/m on scale sizes of a few Debye lengths. A regional-scale hybrid simulation of the

Enceladus plume could possibly incorporate (or at least mimic) these small and intermediate scale electrical effects by adding strong (~0.01-10 V/m) but small-scale quasi-random turbulence to the E-field in the plume region and then determining the efficiency of ion pickup in this more turbulent E-field environment.

Acknowledgements: We gratefully acknowledge NASA's Planetary Science Division and the Cassini Project for enabling this research. The original picket fence idl code creating the data in Figures 3 through12 can be downloaded from the Cassini RPWS web page, http://www-pw.physics.uiowa.edu/cassini/. Instructions for its use are in the opening comments. Any further questions can be directed to WMF.

References

Chen, F. F., (1984), Introduction to plasma physics and controlled fusion: Volume 1 Plasma physics, Plenum press, NY.

Dong, Y., T. W. Hill, and S.-Y. Ye (2015), Characteristics of ice grains in the Enceladus plume from Cassini observations, J. Geophys. Res. Space Physics, 120, 915–937, doi:10.1002/2014JA020288.

Dougherty, M.K. et al., (2006). Identification of a dynamic atmosphere at Enceladus with the Cassini magnetometer. Science 311, 1406–1409.

Farrell, W. M., M. L. Kaiser, J. T. Steinberg, and S. D. Bale (1998), A simple simulation of a plasma void: Applications to Wind observations of the lunar wake, J. Geophys. Res., 103(A10), 23,653.

Farrell, W. M., et al., (2008), Loss of solar wind plasma neutrality and affect on surface potentials near the lunar terminator and shadowed polar regions, Geophys. Res. Lett., 35, L05105, doi:10.1029/2007GL032653.

Farrell, W. M. et al., (2013), The lunar photoelectron sheath: A change in trapping efficiency during a solar storm, J. Geophys. Res. Planets, 118, doi:10.1002/jgre.20086.

Farrell, W. M. et al. (2014), An estimate of the dust pickup currents at Enceladus, Icarus, 239, 217-221.

Goertz, C. K. (1980), Io's interaction with the plasma torus, J. Geophys. Res., 85, 2949.

Goertz, C.K., (1989). Dusty plasmas in the solar system. Rev. Geophys. 27, 271–292.

Gurnett, D.A. et al., (2004). The Cassini radio and plasma wave investigation. Space Sci. Rev. 114, 395. doi:10.1007/s11214-004-1434-0.

Gurnett, D. A., and A. Bhattacharjee, (2005). 'Introduction to plasma physics with space and laboratory applications', Cambridge University Press, Cambridge, UK.

Hansen, C. J., et al. (2006), Enceladus' water vapor plume, Science, 311, 1422.

Hill, T. W., et al. (2012), Charged nanograins in the Enceladus plume, J. Geophys. Res., 117, A05209,ndoi:10.1029/2011JA017218.

Johnson, R. E., et al., 2006, The Enceladus and OH tori at Saturn, Astrophysical. J., 644, L137.

586 Jones, G.H. et al., (2009). Fine jet structure of electrically charged grains in Enceladus'plume.
587 Geophys. Res. Lett. 36, L16204. doi:10.1029/2009GL038284.
588
589 Kriegel, H., et al., (2009) The plasma interaction of Enceladus: 3D hybrid simulations
590 and comparison with Cassini MAG data, Planetary and Space Science, 57, 2113-2122,
591 doi:10.1016/j.pss.2009.09.025.
592
593 Kriegel, H., et al., (2011), Influence of negatively charged plume grains on the structure of
594 Enceladus' Alfven wings: Hybrid simulations versus Cassini Magnetometer data, Journal of
595 Geophysical Research (Space Physics), 116, A10223, doi: 10.1029/2011JA016842.
596
597 Kriegel H., et al. (2014), Ion densities and magnetic signature of dust pickup at Enceladus, J.
598 Geophys Res., Space Physics, 119, 2740-2774.
599
600 Meier, P., (2014), A model of the spatial and size distribution of Enceladus dust plume, Planetary
601 Space Sci., 104, 216-223.
602
603 Morooka, M.W. et al., (2011). Dusty plasma in the vicinity of Enceladus. J. Geophys.
604 Res. 116, A12221. doi:10.1029/2011JA017038.
605
606 Omidi, N., R. L. Tokar, T. Averkamp, D. A. Gurnett, W. S. Kurth, and Z. Wang (2012), Flow
607 stagnation at Enceladus: The effects of neutral gas and charged dust, J. Geophys. Res., 117,
608 A06230, doi:10.1029/2011JA017488.
609
610 Omidi, N., et al., (2010), Hybrid simulations of plasma-neutral-dust interactions at Enceladus, in
611 Pickup Ions Throughout the Heliosphere and Beyond, edited by J. A. le Roux et al., AIP Conf.
612 Proc., 1303, 237–242.
613
614 Pickett, J. S., W. S. Kurth, D. A. Gurnett, R. L. Huff, J. B. Faden, T. F. Averkamp, D. Píša, and
615 G. H. Jones (2015), Electrostatic solitary waves observed at Saturn by Cassini inside 10 R_S
616 and near Enceladus, J. Geophys. Res. Space Physics, 120, 6569–6580, doi:10.1002/
617 2015JA021305.
618
619 Pontius Jr., D.H., and Hill, T.W., (2006). Enceladus: A significant plasma source for Saturn's
620 magnetosphere. J. Geophys. Res. 111, A09214. doi:10.1029/2006JA011674.
621
622 Porco, C.C. et al., (2006). Cassini observes the active south pole of Enceladus. Science
623 311, 1393. doi:10.1126/science.11,23,013.
624
625 Postberg F. et al., (2009), Sodium salts in E-ring ice grains from an ocean below the surface of
626 Enceladus, Science, 459, 1098, doi:10.1038/nature08046
627
628 Shafiq, M. et al., (2011). Characteristics of the dust–plasma interaction near
629 Enceladus' South Pole. Planet. Space Sci. 59, 17–25.
630
631 Spahn, F. et al., (2006). Cassini dust measurements at Enceladus and implications for

the origin of the E-ring. Science 311, 1416. doi:10.1126/science.1121375.

Teolis, B. D., M. E. Perry, B. A. Magee, J. Westlake, and J. H. Waite (2010), Detection and measurement of ice grains and gas distribution in the Enceladus plume by Cassini's Ion Neutral Mass Spectrometer, J. Geophys. Res., 115, A09222,doi:10.1029/2009JA015192.

Tokar, R. L., R. E. Johnson, M. F. Thomsen, R. J. Wilson, D. T. Young, F. J. Crary, A. J. Coates, G. H. Jones, and C. S. Paty (2009), Cassini detection of Enceladus' cold water-group plume ionosphere, Geophys. Res. Lett., 36, L13203, doi:10.1029/2009GL038923.

Wahlund, J.-E., et al. (2009), Detection of dusty plasma near the E-ring of Saturn, Planet. Space Sci., 57, 1795–1806, doi:10.1016/j.pss.2009.03.011.

Waite Jr., J.H. et al., (2006), Cassini Ion and Neutral Mass Spectrometer: Enceladus plume composition and structure. Science 311, 1419. doi:10.1126/ science.1121290.

Waite Jr., J.H. et al., (2009), Liquid water on Enceladus from observations of ammonia and 40Ar in the plume. Nature 460, 487. doi:10.1038/nature081

Table 1. Plasma parameters for E3 Flyby	Langmuir Probe (see Fig 4 Morooka et al.,2011)	Magnetometer/Hybrid model (see Fig 4d of Kriegel et al., 2014)
Ion Density (e/cm^3)	~ 30000	~1500
Electron Density (e/cm^3)	~ -1000	~ - 500 (inferred)
Submicron Grain Charge Density (e/cm^3)	~ - 29000	Not included
Nanoparticle Charge Density (e/cm^3)	Not measured	~ - 1000

Table 1: A comparison of peak plasma values measured by the Cassini RPWS Langmuir Probe and those derived from inversion of the magnetometer data via hybrid codes.

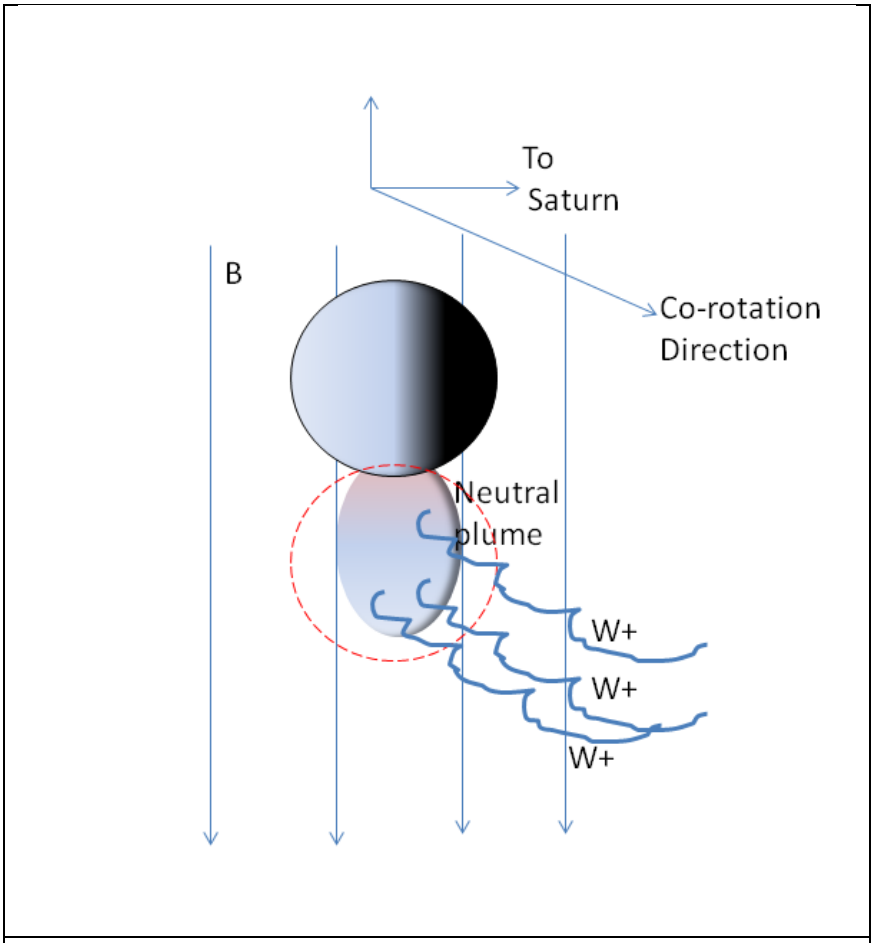

Figure 1 – Illustration of water ions, W+, exiting the plume region via pickup processes.

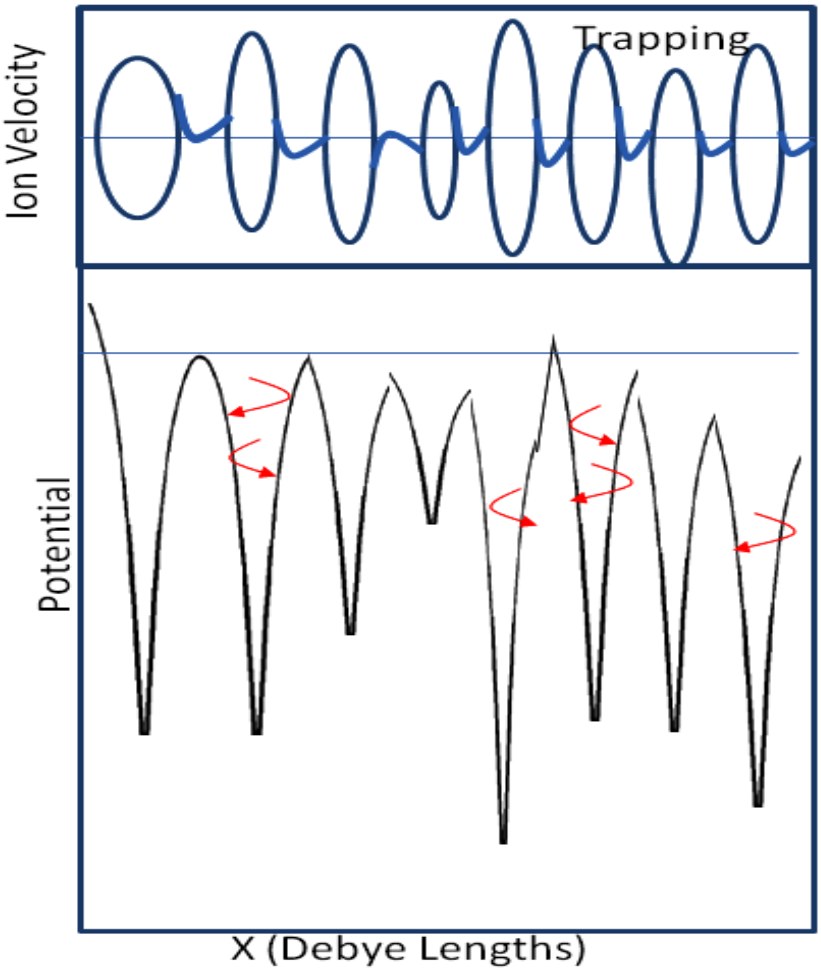

Figure 2 – Illustration of negative charged dust grain potentials (bottom), and the phase space distribution expected for trapped ions in the sheath (top). The blue line represents the location of ions in velocity space. The spatial width of the potentials is a few Debye lengths and the strength of the negative potentials is 5 – 10 V.

725

726

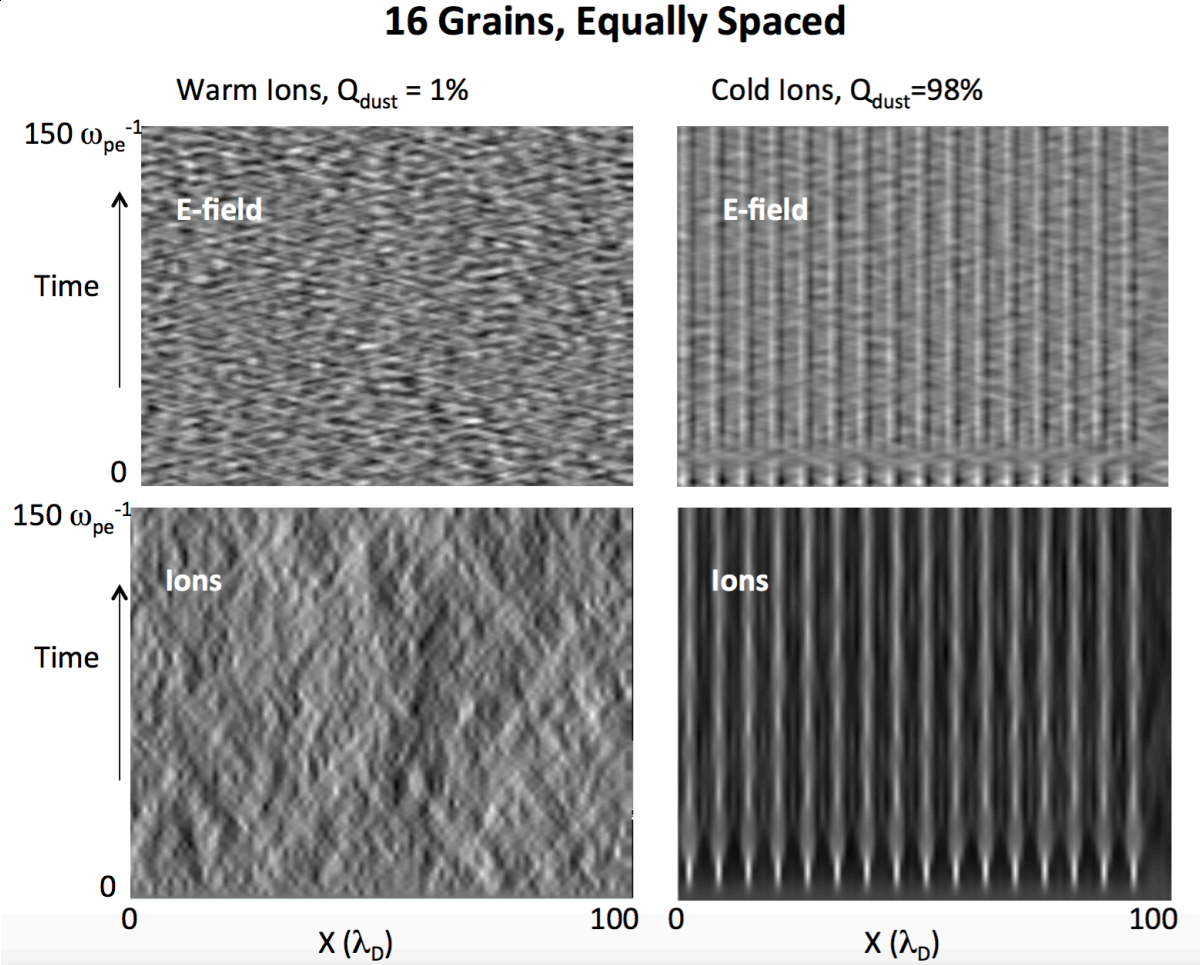

Figure 3- The E-field and ion density x vs t plots for 16 dust grains in the case of (left) warm ions and Q_{dust} absorbing 1% of the local electron population and (right) cold ions and Q_{dust} absorbing 98% of the local electron population. The grey scale is auto-scaled from max to min value, defined with relative enhancement in concentrations appearing as white and relative depletions as black. The greatest concentrations in E and ion density are thus indicated by white and depleted regions indicated by black. Note that the grey scale is automatically adjusted in each figure to the maximum and minimum value for E and density in that plot. This format accentuates the visualization of the concentration of ion bunches, which manifest themselves as local maxima about each dust grain.

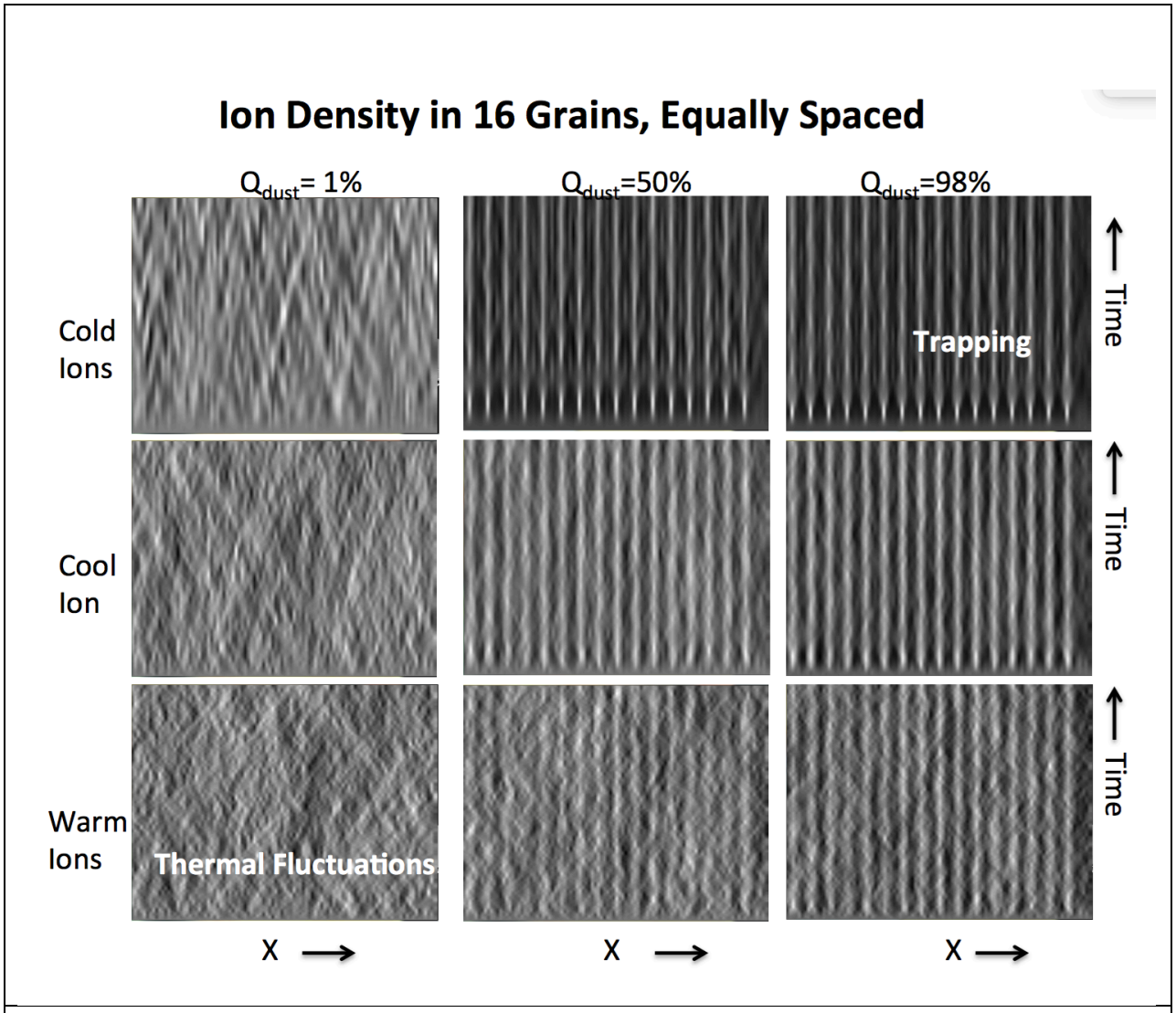

Figure 4- Ion density x-vs-t plots for 9 different simulations runs, each with 16 equally-spaced dust grains but with varying dust charge state and ion temperature. In each panel, X ranges over 0 to 100 Debye lengths and time increase from 0 to 150 plasma periods.

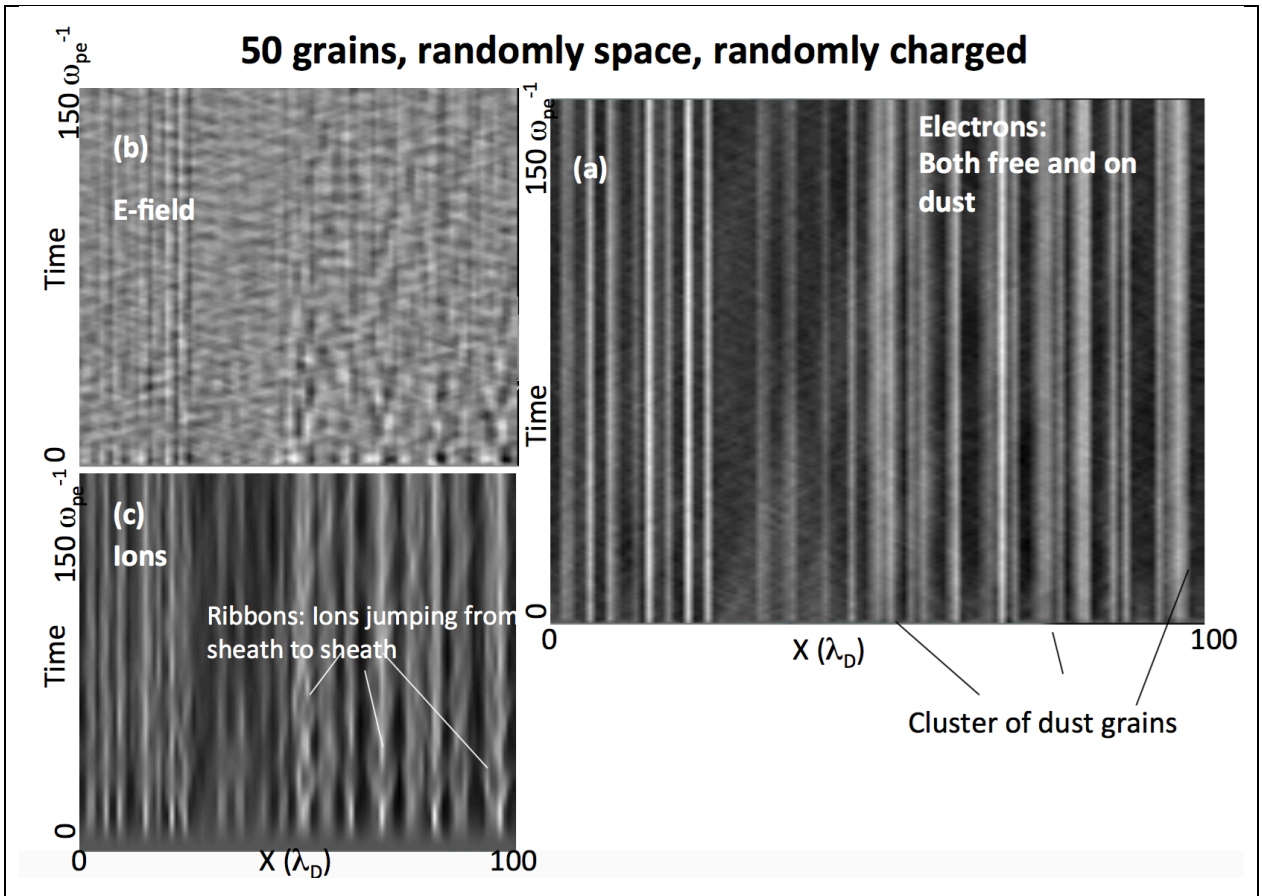

Figure 5- Simulation results for 50 randomly spaced and randomly charged negative dust grains, with (a) negative charge concentrations (i.e., grain locations), (b) E-field, and (c) positive ion charge concentrations.

743
744
745
746
747
748

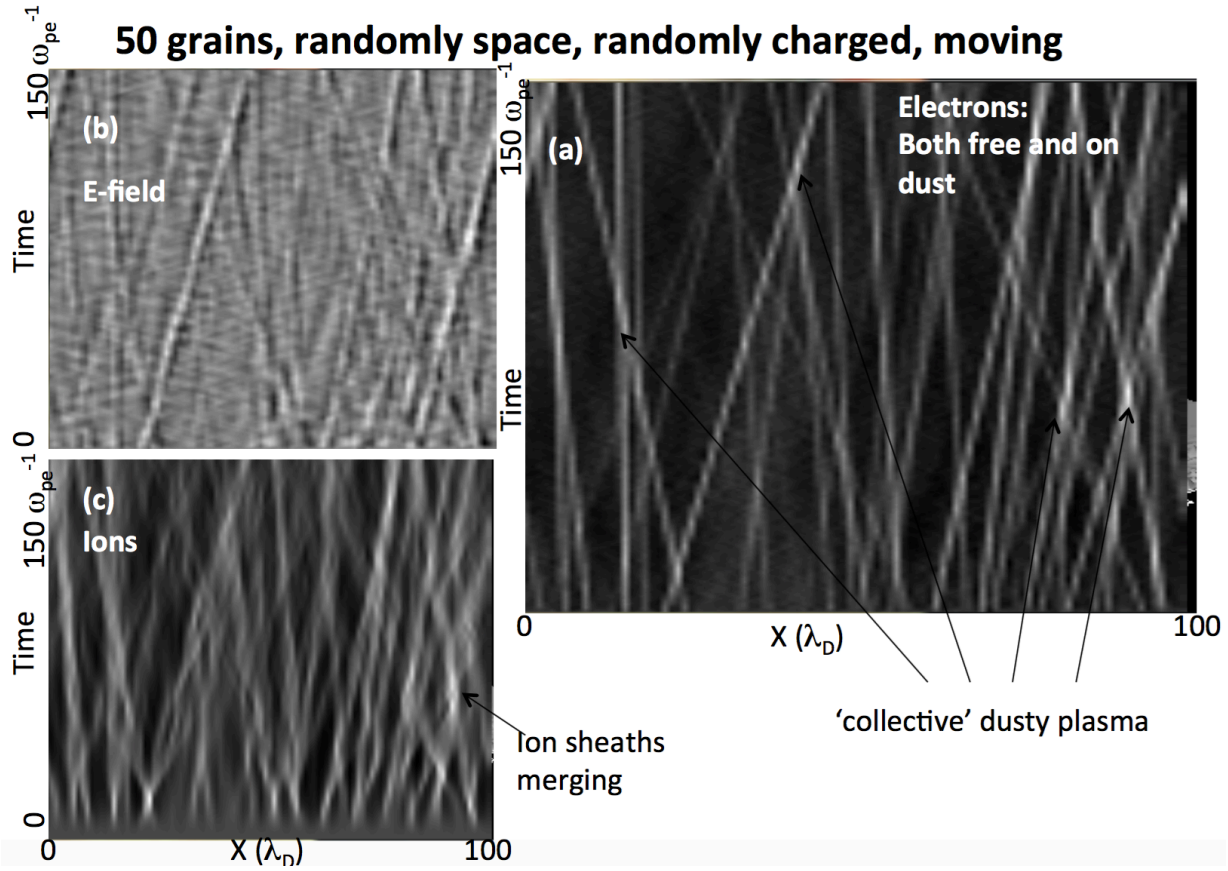

Figure 6- Simulation results for 50 randomly spaced and randomly charged negative mobile dust grains, with (a) negative charge concentrations (i.e., grain locations), (b) E-field, and (c) positive ion charge concentrations.

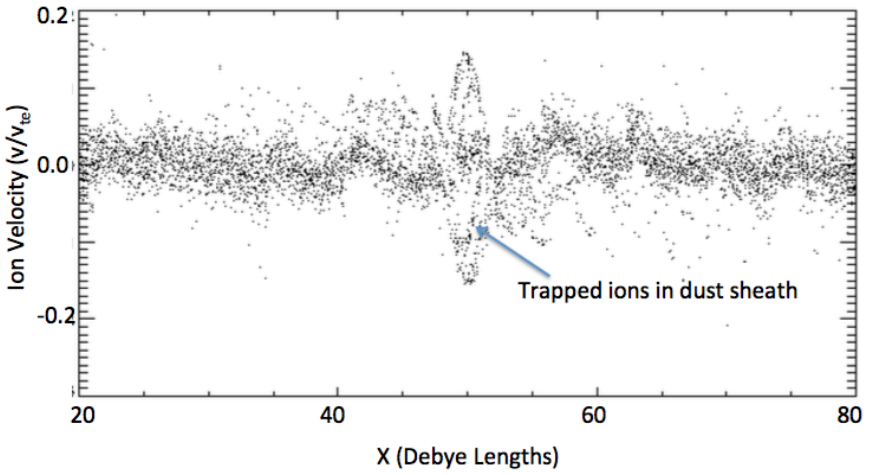

Figure 7- The ion phase space distribution at t= 200 plasma periods for a singe charged grain. Note the development of water-bag trapping structures in dust grain potential wells.

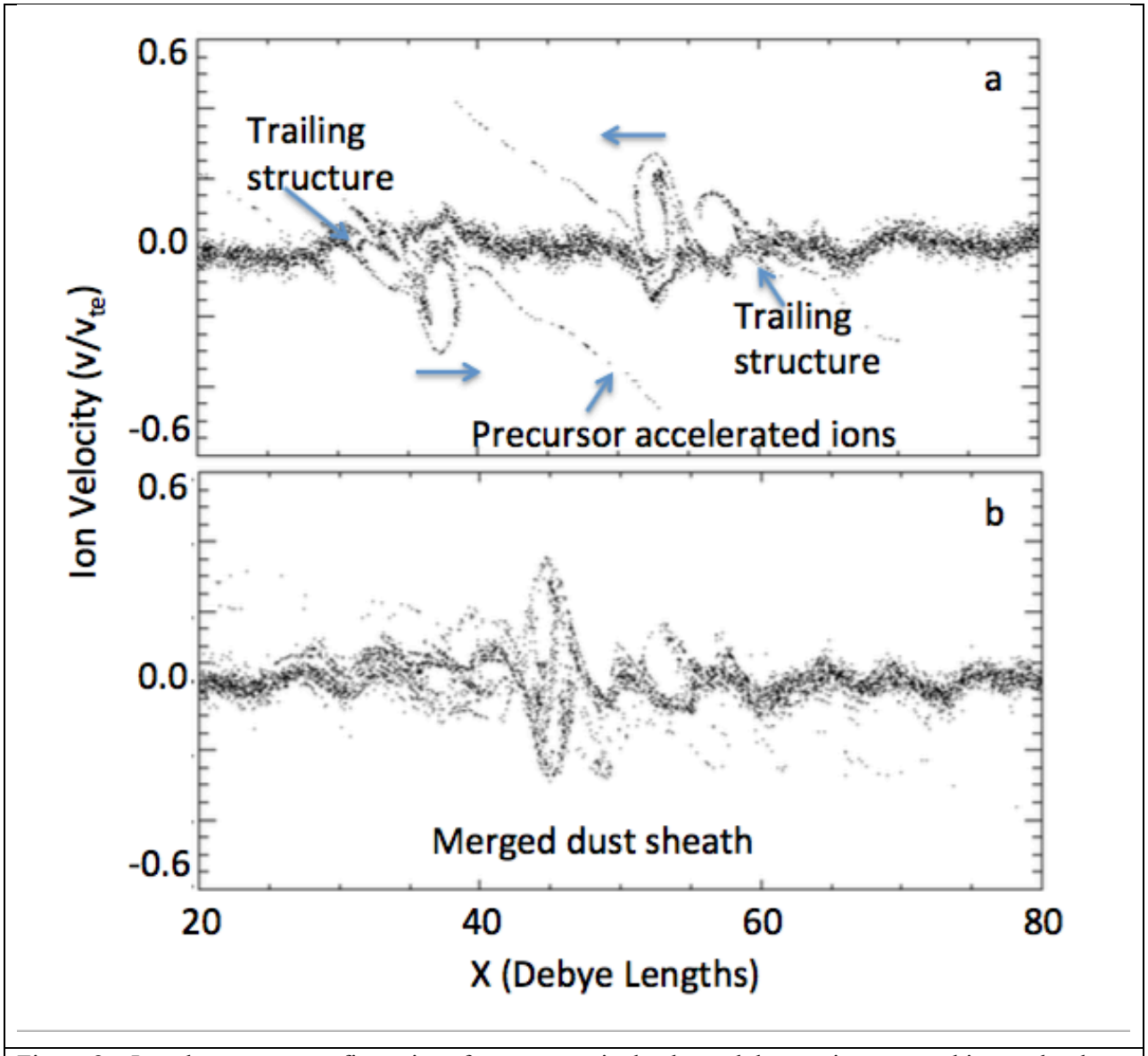

Figure 8 – Ion phase space configurations for two negatively charged dust grains approaching each other at 0.15 V_{te}. Note in (a) that each grain traps its own set of ions forming an ion sheath. When the grains merge 9b), the ions in each sheath also merge and the once-isolated populations are allowed to interact.

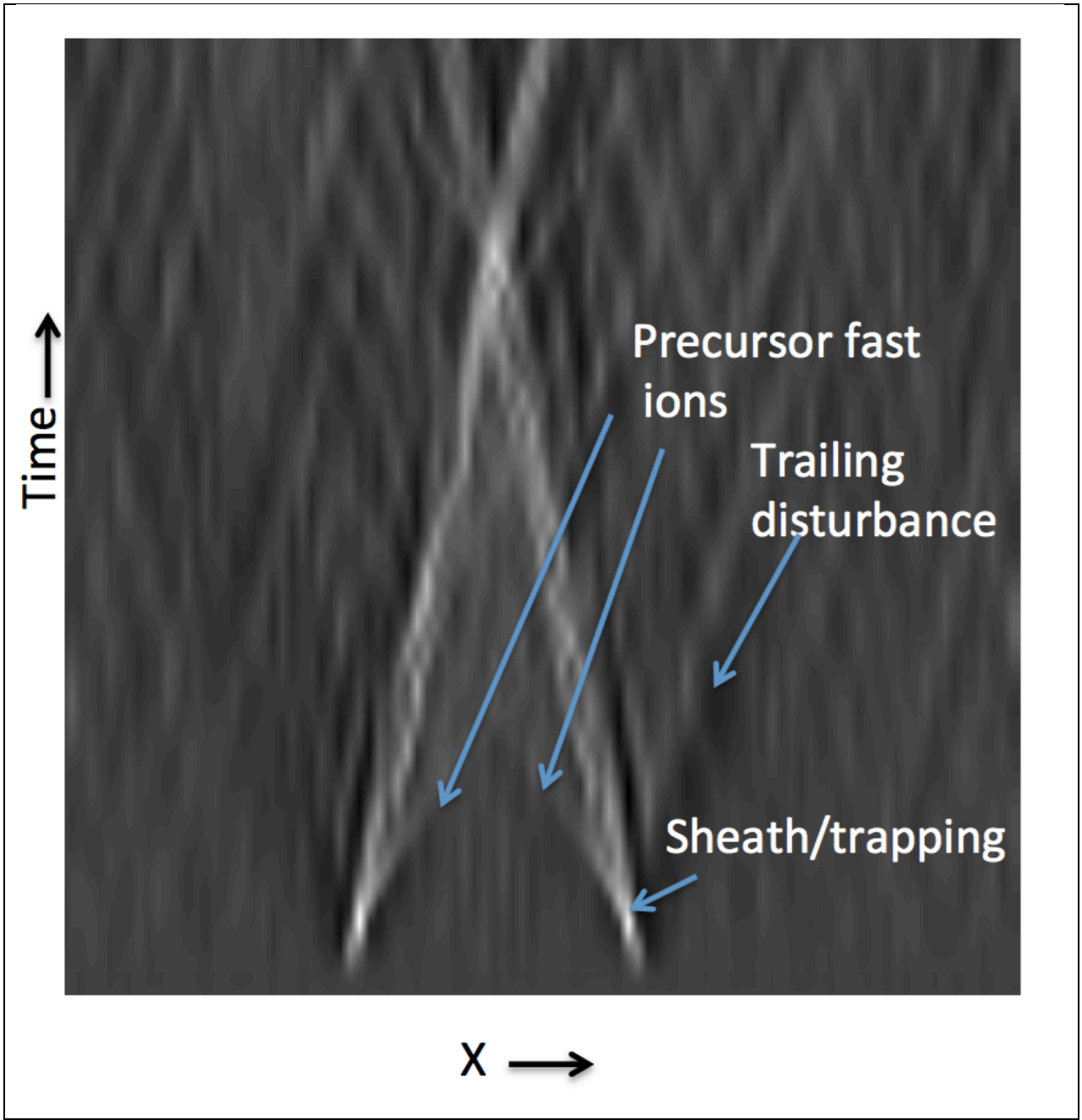

Figure 9- The ion density as a function of position (100 Debye lengths) and time (200 plasma periods) for the case run in Figure 8. While the ions are initially free, those in the vicinity of the charged dust are attracted to the dust potentials to form sheaths. These sheaths interact where the grains trajectories intersect.

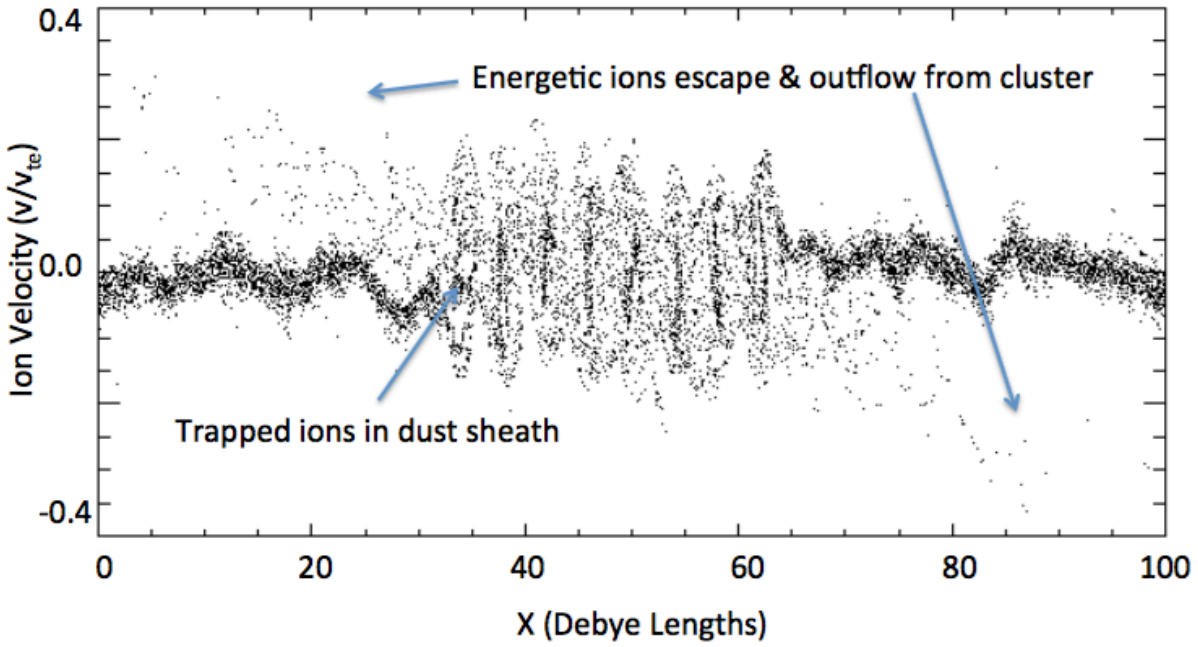

Figure 10 – The phase space distribution of ions that form about a dust cluster consisting of 8 negatively charged grains each separated by 4 Debye lengths. Note the formation of phase space 'water-bag' structures associated with ion trapping.

778

779

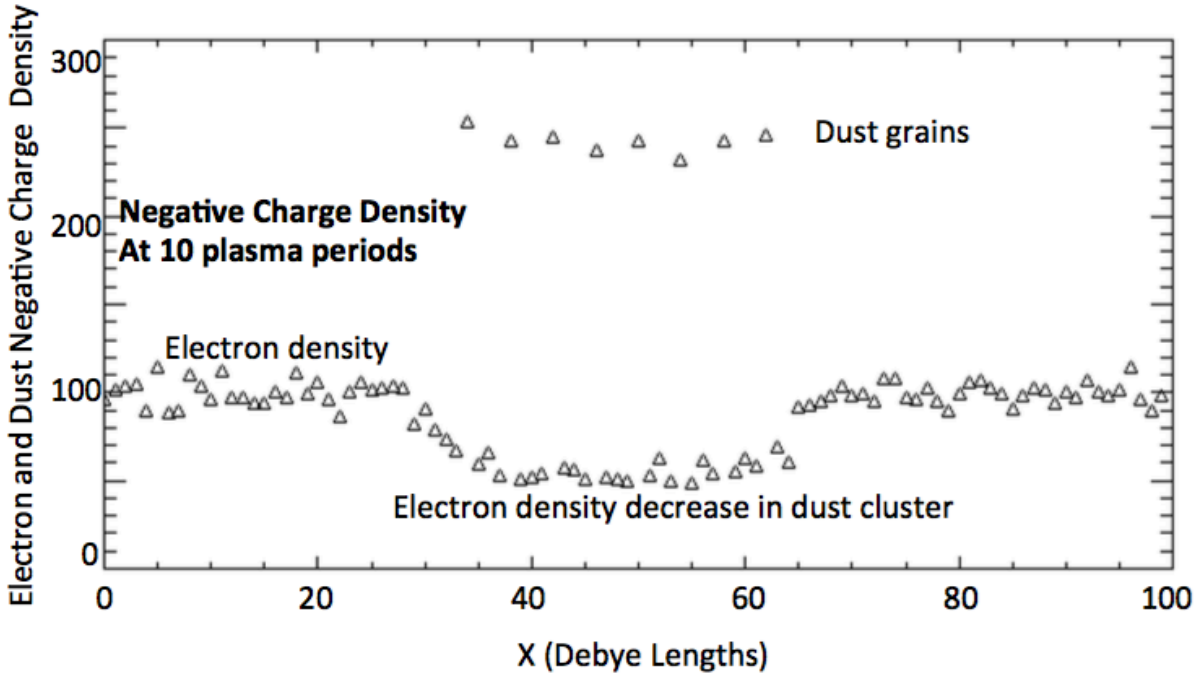

Figure 11- The electron distribution for the case run in Figure 10. Within the cluster, the electron density is decreased in order to maintain neutrality with the negative dust grains and ions across the simulation box. The simulation was purposely designed to take the electrons from the plasma and place them on the dust (or in bunches) thereby ensuring this neutrality.

780

781

782

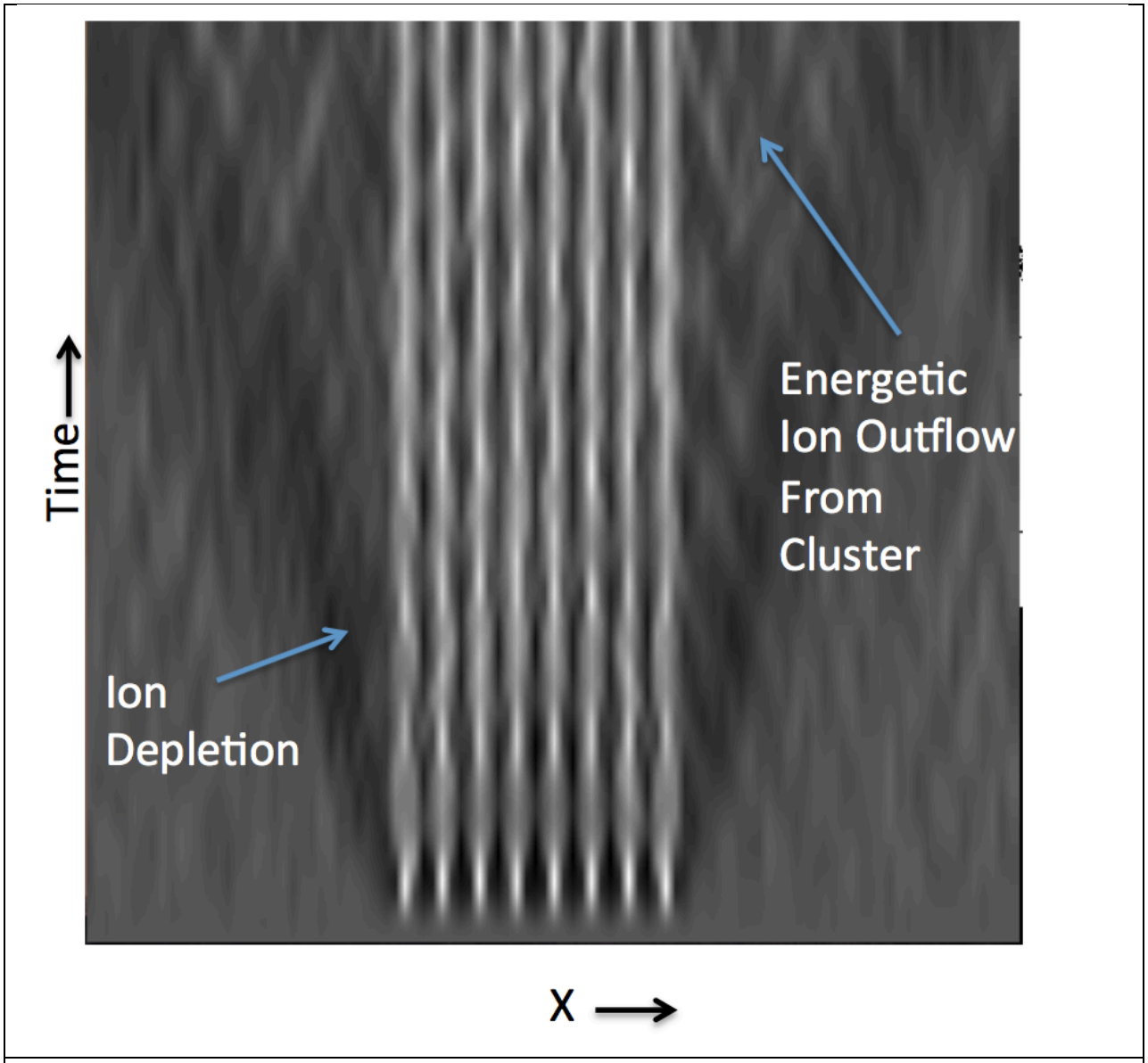

Figure 12 – The ion density as a function of position (100 Debye lengths) and time (200 plasma periods) for the cluster case run in Figure 10. While the ions are initially free, those in the vicinity of the charged dust are attracted by the dust potentials to form sheaths.

792